Article

Single-molecule mass measurements reveal distinct effects of sodium and potassium on mini-spidroin assembly

Check for updates

Hannah Osterholz [1], Shree Senthil Jeyalekshmy [1], Benjamin Schmuck [2], Tomas Bohn Pessatti [2], Justin L. P. Benesch[3,4], Anna Rising[2,5] ✉, Axel Leppert [1] ✉ & Michael Landreh [1,6] ✉

Spider silk formation involves tightly regulated protein assembly influenced by pH and the presence of ions. Kosmotropic salts induce phase separation of spidroins; however, their exact role in assembly is not clear. Here, we investigate how sodium and potassium phosphate affect spidroin interactions via the single-molecule method of mass photometry. We observed that spidroin oligomerization occurs at low nanomolar protein concentrations. Potassium ions were found to stabilize a compact conformation of individual spidroins and slow down pH-induced β-sheet aggregation, consistent with its more kosmotropic nature. Microfluidic MP showed that pre-assembly of the protein through salt-induced phase separation reduced the number and size of oligomeric intermediates that form upon acidification. Together, the findings suggest that spidroins have an inherent ability to self-assemble, blurring the line between one- and two-phase status. Subtle differences in ion composition are sufficient to change spidroin stability and assembly, potentially contributing to silk spinning in vivo by balancing storage stability with rapid fiber formation.

Spider silk is an extraordinary biomaterial due to its high tensile strength, extensibility, and biocompatibility. The primary protein components of spider silk are spidroins, highly dynamic proteins with a long, mostly disordered repeat region flanked by non-repetitive C- and N-terminal domains (Fig. 1a)[1,2]. Spidroins undergo a complex and highly regulated assembly process during silk fiber formation. They are stored in the silk gland as a highly concentrated, soluble dope[3,4]. During spinning, the dope is extruded through a narrowing duct while experiencing shear forces and a pH drop from pH >7 to *ca.* pH 5 (Fig. 1b)[4,5]. Acidification induces antiparallel dimerization of the N-terminal domain (NT), which cross-links the spidroins[6–8]. The C-terminal domain (CT) is a constitutive dimer, which is in some spidroins linked by a disulfide bond[9]. Each subunit contains a conserved salt bridge that is broken at low pH to initiate β-sheet aggregation[5,9]. Using engineered mini-spidroins composed of the terminal domains as well as a repetitive domain with two repeats (NT2RepCT), it was shown that the pH-induced structural changes in the NT and CT domains trigger the conversion of the soluble protein into solid fibers[10,11].

Another contributing factor in spidroin assembly is the presence of various ions in the silk gland. The sac of the gland contains high amounts of sodium and chloride (192 and 164 mM, respectively), which are exchanged for potassium and phosphate in the spinning duct (Fig. 1b)[5,12]. Native major ampullate spidroins as well as recombinant mini-spidroins can undergo liquid-liquid phase separation (LLPS) in vitro when exposed to high concentrations (>250 mM) of phosphate[13–16]. Phase separation is driven by low-affinity interactions between poly-alanines as well as aromatic and basic residues in the repeat domains, giving rise to liquid-like macroscopic droplets[14,15,17]. LLPS has a pronounced effect on the aggregation behavior of NT2RepCT, shifting from being stable at neutral pH to spontaneously converting into β-sheet-rich aggregates within hours[14,18]. This destabilizing effect is mediated by the CT domain, which contains an N-terminal disordered extension capable of LLPS[9,14]. Inducing LLPS of the extended CT domain strongly accelerates the conversion to β-sheet at low pH, whereas removal of the extension renders CT insensitive to LLPS conditions[14]. NMR studies have furthermore shown that ions affect the structure of the repeat domain, with chaotropic ions favoring a random coil conformation, whereas kosmotropic ions promote turn and helix formation[19]. Together, the observations suggest that kosmotropic ions tune LLPS-like

[1]Department for Cell and Molecular Biology, Uppsala University, Uppsala, Sweden. [2]Department of Animal Biosciences, Swedish University of Agricultural Sciences, Box 7023, Uppsala, Sweden. [3]Department of Chemistry, University of Oxford, Physical and Theoretical Chemistry Laboratory, Oxford, UK. [4]Kavli Institute for Nanoscience Discovery, Biochemistry Building, Oxford, UK. [5]Department of Medicine Huddinge (MedH), Karolinska Institutet, Neo, Huddinge, Sweden. [6]Department of Microbiology, Tumor and Cell Biology, Karolinska Institutet, Solna, Sweden. ✉e-mail: anna.rising@slu.se; leppert@icm.uu.se; michael.landreh@icm.uu.se
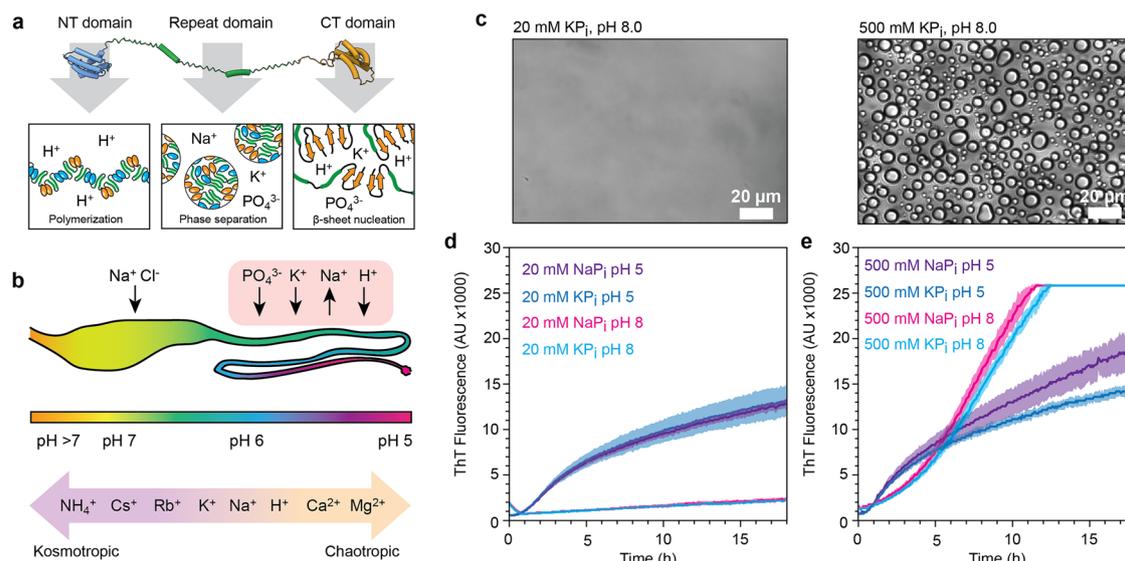
Fig. 1 | Spidroin- and silk gland architecture and salt- and pH-induced aggregation of NT2RepCT[YF]. a Structure of the NT2RepCT mini-spidroin. The NT domain (blue) undergoes dimerization below pH 6. The repeat domain (green) composed of two poly-alanine segments and disordered linkers drives LLPS in the presence of NaP$_i$ or KP$_i$. The CT domain (yellow) is a constitutive dimer and undergoes β-sheet aggregation when exposed to acidic pH or high NaP$_i$ or KP$_i$ concentrations. **b** Architecture of the silk gland. The spinning dope is stored in the sac at pH 7-8, but undergoes acidification to pH 5, as well as increased phosphate and potassium concentrations, during passage through the spinning duct. The

Hofmeister series for cations is shown below. **c** Light microscopy of NT2RepCT[YF] shows droplet formation in the presence of 500 mM KP$_i$. **d** ThT fluorescence shows that pH-induced aggregation of NT2RepCT[YF] is near-identical in 20 mM KP$_i$ and 20 mM NaP$_i$. **e** ThT assays of NT2RepCT[YF] in 500 mM phosphate buffer show pronounced aggregation at pH 8 and rapid aggregation accompanied by reduced ThT fluorescence at pH 5. At pH 5 and 500 mM phosphate buffer, sodium increases aggregation compared to potassium. Lines and shaded areas indicate the average and standard deviation, respectively, of three repeats.

interactions as part of the spinning process, although their exact concentrations in the gland have not been established[20].

While the kosmotropic nature of phosphate has been shown to be important for spidroin LLPS, the roles of sodium and potassium are less established. Both have similar Hofmeister properties, with potassium being only slightly more kosmotropic than sodium (Fig. 1b), and potassium and sodium phosphate buffers are similarly efficient at inducing spidroin LLPS in vitro[13,15]. The fact that the spider removes sodium and increases the potassium content of the dope during spinning thus raises the question whether both may affect spidroins differently[12].

Here, we employed mass photometry (MP) to unravel how different ion and pH regimes affect the interactions of the NT2RepCT mini-spidroin at the single-molecule level. We find that low concentrations of potassium, but not sodium, suppress oligomerization by stabilizing spidroin dimers in the dilute phase. Microfluidic rapid-mixing MP reveals that exposure of spidroins to potassium phosphate prior to pH-induced assembly reduces oligomeric intermediates compared to sodium phosphate. Our findings show that mini-spidroins interact at nanomolar concentrations, and that these interactions are modulated by sodium and potassium, which may help to control the formation of spidroin clusters.

Results
Potassium affects LLPS-induced aggregation of NT2RepCT[YF]
To study the combined effects of phosphate salt and pH, we used a variant of NT2RepCT, where two tyrosines in each repeat were replaced with phenylalanine (NT2RepCT[YF])[21]. Compared to NT2RepCT, NT2RepCT[YF] more forms larger, more dynamic droplets when exposed to 500 mM sodium or potassium phosphate. The increased LLPS propensity enables the study of spidroin droplet formation despite the low number of repeats (Fig. 1c)[14]. As a first step, we investigated how the combinations of high and low phosphate buffer concentrations and high and low pH affect spidroin aggregation, using the β-sheet-sensitive fluorescent dye Thioflavin T (ThT). Exposure of NT2RepCT[YF] to pH 8 in the presence of 20 mM NaP$_i$ or KP$_i$ resulted in no change in ThT fluorescence. Lowering the pH to 5 caused a rapid increase in

fluorescence, as expected for aggregation triggered by the NT and CT domains (Fig. 1d)[5]. Under LLPS conditions (500 mM NaP$_i$ or KP$_i$)[14,15], we observed a strong increase in fluorescence at pH 8 (Fig. 1e), with KP$_i$ being slightly slower than NaP$_i$. These findings are in good agreement with the reported slow conversion of droplets into β-sheet spherical aggregates[18]. We then tested lowering the pH in addition to inducing LLPS by exposing the spidroins to a combination of 500 mM phosphate buffer and pH 5. We observed a more rapid fluorescence increase than at pH 8, suggesting that pH-induced aggregation superseeds aggregation at high phosphate concentration. Interestingly, 500 mM NaP$_i$ led to a greater fluorescence increase than KP$_i$. This finding suggests that at high salt concentrations, sodium promotes spidroin aggregation more efficiently than potassium. Light microscopy before and after 18 h incubation at 30 °C showed the formation of amorphous aggregates after incubation at pH 5 under low salt conditions. After incubation under high salt conditions, the spidroins gelated as partly fused droplets, which appeared smaller if the pH was additionally lowered to 5 (Fig. S1).

Potassium reduces oligomer formation at nanomolar protein concentrations
To investigate whether NaP$_i$ and KP$_i$ ions affect the interactions of mini-spidroins under assembly conditions, we turned to mass photometry (MP), which measures the molecular weight of proteins in solution based on their light scattering properties[22]. Importantly, MP typically operates at protein concentrations in the low nanomolar range, well below the threshold for NT2RepCT[YF] spinning or LLPS[10,15,23]. Therefore, it enables us to monitor how assembly states are impacted by high and low pH, as well as by low and high salt concentrations, without bias that could arise from protein partitioning into dilute and dense phases. For MP measurements, a 10 μM stock of NT2RepCT[YF] in MQ was diluted to 400 nM in different buffers, equilibrated for a minimum of 2 minutes, and subsequently loaded into the mass photometer sample chamber at a final concentration of 20 nM (Fig. 2a). In 20 mM NaP$_i$ at pH 8 (Fig. 2b, pink), we observed NT2RepCT[YF] dimers (66 kDa) as the dominant species. We also detected oligomers of dimers,
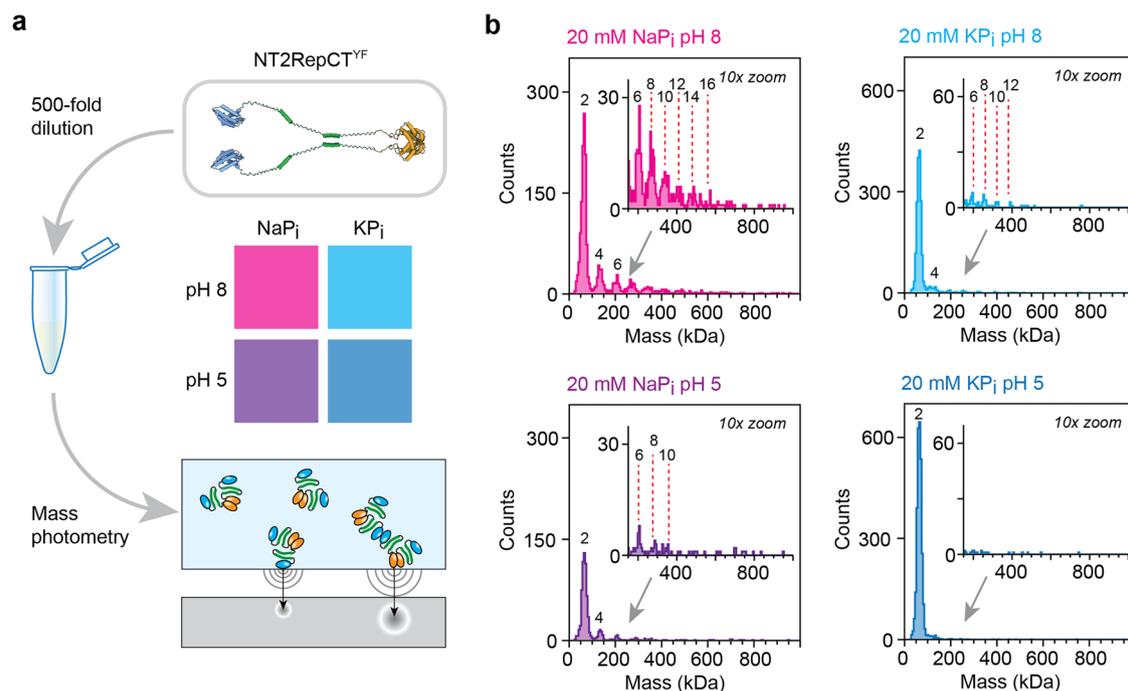
Fig. 2 | Low concentrations of potassium suppress NT2RepCT^YF oligomerization. (a) Experimental strategy for steady-state MP. NT2RepCT^YF is diluted 500 times in NaP_i or KP_i buffer prior to MP measurements. (b) MP histograms show oligomers of dimers up to 16-mers in NaP_i at pH 8 (pink histogram). The signal intensity decreases in NaP_i at pH 5 (purple histogram). In the presence of KP_i, fewer oligomers are detected at pH 8 (light blue histogram), and none at pH 5 (dark blue histogram). Theoretical molecular weights and oligomeric states are indicated by red dashed lines.

which could be resolved up to the 462 kDa 14-mer (Fig. 2b, pink insert). When the protein was diluted in 20 mM NaP_i at pH 5, the total count of events decreased by *ca.* 50%. This finding indicates loss of protein from the solution, which is consistent with pH-induced aggregation. Despite the reduced signal, spidroin oligomers up to a decamer (330 kDa) could again be observed, with the ratios between dimers and oligomers largely unchanged (Fig. 2b, purple). When the experiment was repeated with KP_i, only minor oligomerization of dimers was observed at high pH, both in terms of signal intensity and oligomer size (Fig. 2b, light blue insert). Lowering the pH to 5 resulted in an increase in NT2RepCT^YF dimer signal and a near-complete loss of oligomers. Upon raising the salt concentration to 500 mM, no other assembly states than dimers were observed, both at low and high pH, as well as with NaP_i and KP_i (Fig. S2). We conclude that low amounts of potassium reduce the formation of NT2RepCT^YF oligomers both at low and high pH compared to sodium. High sodium or potassium phosphate concentrations, on the other hand, generally favor the dimeric state of NT2RepCT^YF under MP conditions.

To gain more insights into how low concentrations of sodium and potassium affect NT2RepCT^YF conformations, we turned to native ion mobility mass spectrometry (IM-MS). Here, electrospray ionization (ESI) is used to transfer intact protein complexes from solution to the gas phase and the confirmation of the ions is analyzed by measuring the time it takes them to traverse a gas-filled drift cell[24]. Although ESI relies on volatile buffers to produce ions, it tolerates low millimolar concentrations of non-volatile salts[25]. This feature of nMS has been used to study the effect of salts in the Hofmeister series on the conformations and stabilities of protein complexes[26]. We therefore recorded positive ionization mode mass spectra of 10 μM NT2RepCT^YF in 100 mM ammonium acetate, which is commonly used to stabilize protein complexes during ESI. The solution was supplemented with either 10 mM sodium acetate or potassium acetate, as phosphate buffers cause signal suppression. We then compared the arrival times of the 11+ to 13+ charge states of the monomer as well as the 19+ charge state of the dimer. These charge states were clearly discernible for all three conditions, facilitating comparison of their ion mobilities. The resulting arrival time distributions show that under otherwise identical conditions, the protein retains a more compact conformation in the presence of potassium compared to sodium, both in its monomeric and dimeric state, as well as with bound sodium or potassium ions. The highest monomer charge state that was detectable in all conditions contains a partially extended population, which was most prominent in the presence of sodium ions, indicating increased unfolding (Figure S3). These data indicate that protein oligomerization observed by MP coincides with a less compact conformation as seen by IM-MS.

Potassium and sodium affect self-association of the repeat domains

To gain insight into the contributions of the different domains of NT2RepCT^YF to oligomerization, we performed the same MP experiments with NT2Rep, which lacks the CT domain (Fig. 3a), and the isolated NT domain (Fig. 3b). Both proteins are too small to be detected as monomers (NT2Rep: 22 kDa, NT: 15 kDa) but can be detected in their dimeric states, since MP has a lower mass limit of approximately 30 kDa[23]. While not informing about the monomer/dimer ratio, the data reveal that a fraction of the protein is dimeric even at high pH. In 20 mM NaP_i, pH 8, the dimer peak for NT2Rep showed a broad higher-mass shoulder, which was poorly resolved, suggesting the presence of oligomers that range in size up to ca. 10 monomers (Fig. 3a, pink histogram). At pH 5, the intensity of the dimer peak increased a bit, and the shoulder peak persisted, but could be better resolved into tetramers, hexamers, and octamers (Fig. 3a, purple histogram). We speculate that the increased resolution is due to the oligomers being composed mainly of dimers (44 kDa). In 20 mM KP_i we observed exclusively dimers and no higher oligomers (Fig. 3a, light blue and dark blue histograms). When repeating the same experiment with NT, only dimers were detected (Fig. 3b). The NT dimer (30 kDa) is at the lower detection limit of the instrument and was not used for quantification. The histograms showed no notable differences between NaP_i and KP_i and no higher NT oligomers. MP of NT2Rep or NT in 500 mM NaP_i or KP_i showed an
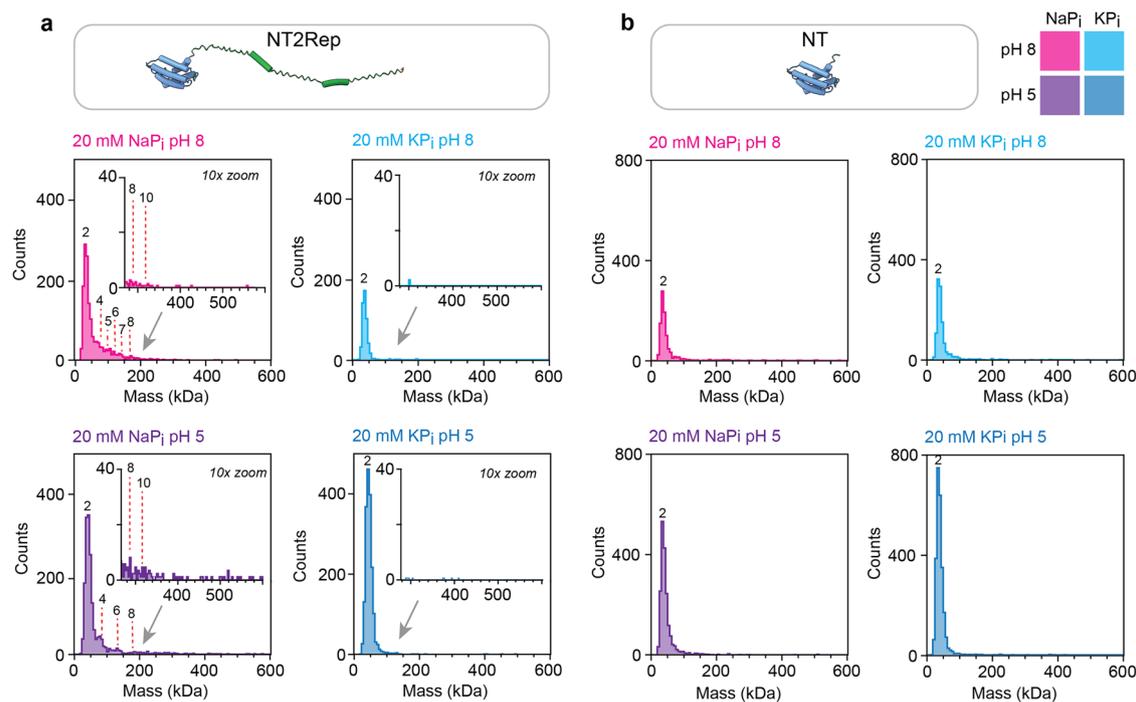
Fig. 3 | NT2Rep, but not NT, oligomerizes in a potassium-sensitive manner. a MP histograms of NT2Rep at pH 8 (top row) or 5 (bottom row) show poorly resolved oligomers in the presence of 20 mM NaP$_i$. The oligomers are slightly better resolved at pH 5 than at pH 8. No oligomers are detected in KP$_i$. **b** Histograms of the NT domain dimer show no major differences between NaP$_i$ and KP$_i$ buffers. Theoretical molecular weights and oligomeric states are indicated by red dashed lines.

increase in dimers at pH 5 but otherwise no differences between conditions (Fig. S4).

The finding that NT2Rep, but not NT, forms oligomers in 20 mM NaP$_i$ indicates that self-association is to a significant extent mediated by the repeat domains, and NT dimerization may contribute by increasing the number of repeats per complex. NT2RepCT^{YF} contains four repeat domains per dimer, which may account for the higher signal intensity of the oligomers formed by the full-length mini-spidroin (Figs. 3a, 2b). Together, the data imply that at low ion and protein concentrations, KP$_i$ reduces oligomerization of repeat domains by promoting a compact conformation.

Inducing LLPS suppresses NT2RepCT^{YF} assembly intermediates

A consideration when using MP to study spidroin assembly is the requirement to work in dilute solutions[23,27]. As shown above, KP$_i$ reduces oligomerization of NT2RepCT^{YF} at nanomolar protein concentrations. At micromolar protein concentrations, on the other hand, KP$_i$ promotes protein interactions and LLPS, which is a common feature of several spider and silkworm fibroins[14,15,28]. We therefore asked whether we could adapt MP to be able to study the effects of KP$_i$ on NT2RepCT^{YF} assembly under LLPS conditions while circumventing the need for micromolar protein concentrations required for LLPS[29]. We therefore turned to the MassFluidix system (Refeyn, Oxford, UK), which was designed to facilitate analysis of more concentrated solutions by including a rapid dilution step prior to data acquisition[27]. Briefly, the protein solution in buffer A is diluted in buffer B, followed by a 37 millisecond mixing time, and then measured in an MP flow cell[27]. We adapted this system for analysis of spidroin assembly by preparing 10 μM of NT2RepCT^{YF} in LLPS- or non-LLPS buffer at pH 8 and diluting either solution 1000-fold in 20 mM NaP$_i$ at pH 5 to trigger assembly (Fig. 4a). Since NT dimerizes on the low-millisecond timescale[30], we hypothesized that this setup could capture polymerization intermediates of NT2RepCT^{YF}.

First, we analyzed NT2RepCT^{YF} under non-LLPS conditions using 20 mM NaP$_i$ pH 8, as buffer A and B. The resulting histograms have lower

signal intensity than those obtained at steady-state conditions (Fig. 2), and show mostly dimers with a minor fraction of higher oligomers (Fig. 4b, pink histogram). Next, we rapidly lowered the pH by using 20 mM NaP$_i$ pH 5, as buffer B. Strikingly, we observed a wide distribution of oligomeric states, ranging up to the megadalton range, whose intensity decayed exponentially with increasing molecular weight (Fig. 4b, purple histogram). The oligomeric states could not be resolved. Since low pH destabilizes the noncovalent CT dimer, and trimers and pentamers of mini-spidroins have been observed by nMS at pH 5[31], the poor resolution might stem from the presence of even and odd oligomer stoichiometries. As these oligomers are not present in MP histograms recorded under steady-state conditions (Fig. 2), they likely represent assembly intermediates that form within milliseconds and subsequently escape the detection window by becoming too large, too polydisperse, or both.

Next, we induced LLPS prior to diluting the protein for MP measurements, mimicking the proposed events in the gland[20]. When 10 μM of NT2RepCT^{YF} in 500 mM KP$_i$, pH 8 (buffer A, see Fig. 1c) was diluted in 20 mM NaP$_i$, pH 8 (buffer B), the MP histogram showed no pronounced difference compared the data obtained in 20 mM NaP$_i$ only (Fig. 4b, light blue histogram). When the pH was rapidly lowered to 5, we observed no oligomerization, but instead a pronounced reduction in signal intensity (Fig. 4b, dark blue histogram). These data contrast the observation made for non-LLPS conditions, and allow us to delineate a role for LLPS during spidroin assembly: In 20 mM NaP$_i$, pH 8, most spidroins are in the dilute phase. Lowering the pH to 5 causes polymerization via the NT domains, and we can observe a wide range of oligomeric states immediately afterwards. In 500 mM KP$_i$, the proteins form liquid droplets that are held together by weak interactions between the repeat domains. When the pH is lowered to 5, these pre-assembled proteins immediately polymerize into oligomers that are too large for the detection window of the mass photometer. Assuming that NT dimerization is faster than droplet dissolution in the mixing capillary, low pH crosslinks the spidroins while they are closer
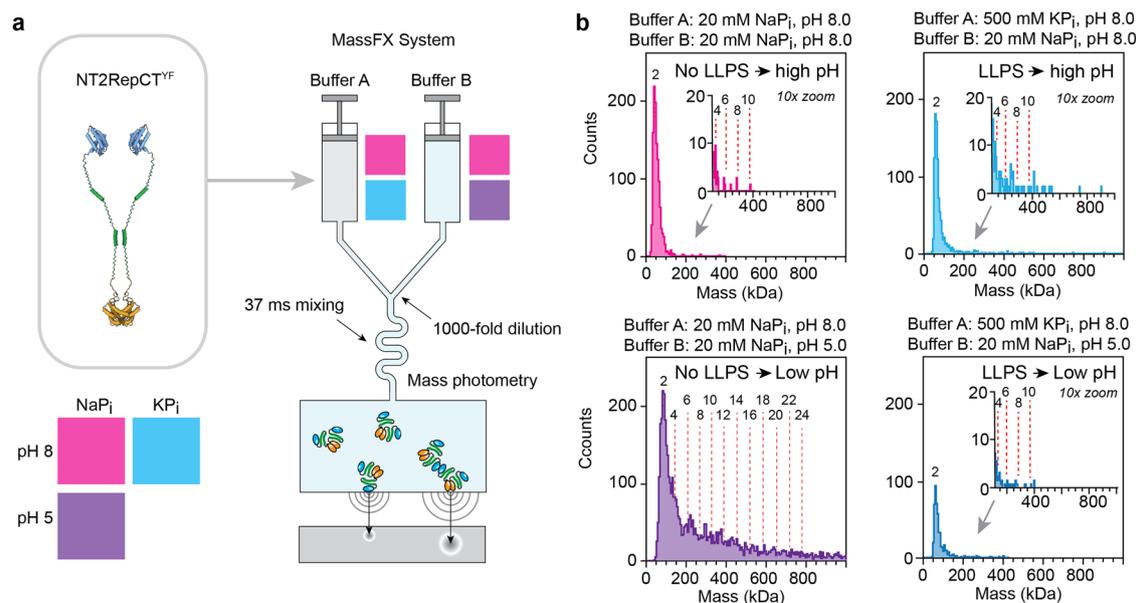
Fig. 4 | Microfluidic MP captures the effect of LLPS on NT2RepCT^YF assembly intermediates. a Architecture of the MassFluidix system. A 10 μM solution of NT2RepCT^YF in non-LLPS or LLPS buffer (buffer A) is rapidly diluted 1000-fold in 20 mM NaP_i buffer at pH 8 or pH 5 (buffer B), and measured in an MP flow cell following 37 ms mixing time. **b** MP histograms of NT2RepCT^YF diluted from non-LLPS buffer (pink and purple histograms) show that lowering the pH to 5 induces broad oligomerization. When NT2RepCT^YF is diluted from LLPS-buffer (light blue and dark blue histograms), lowering the pH results in loss of signal and no detectable oligomers. Theoretical molecular weights and oligomeric states are indicated by red dashed lines.

in space, which we speculate gives rise to larger assemblies in a shorter time frame.

Discussion

Reproducing spinning conditions and monitoring their effects on spidroins at the molecular level is a major challenge in the experimental investigation of spider silk. Here, we have employed MP to investigate the effects of sodium and potassium phosphate, which are present in the silk gland, on the oligomeric state of the NT2RepCT^YF mini-spidroin. MP is a single-molecule technique that can trace individual protein interactions, but requires nanomolar protein concentrations that do not represent native or biomimetic spinning conditions[32]. However, using microfluidics to rapidly switch solution conditions and protein concentrations, we were able to directly observe how ions and pH synergistically affect spidroin assembly.

The data from MP indicate different effects of sodium and potassium on NT2RepCT^YF that are consistent with their positions in the Hofmeister series. Potassium ions, which are slightly kosmotropic, reduce self-association of the repeat domains and stabilize NT2RepCT^YF dimers. The slightly chaotropic sodium ions destabilize the protein and enable intermolecular interactions between the repeat domains. Both cations are close to the middle of the Hofmeister range, yet the fact that we observe effects at low ion concentrations suggests that the partially structured repeat domain may be sensitive to such subtle differences, or engage in ion-specific interactions. Native spidroins contain hundreds of repeats that mediate LLPS[33,34] and therefore may render them more susceptible to minor changes in ion composition. Here, the potassium-induced compaction of individual spidroins that we observe at nanomolar protein concentrations likely stems from increased intramolecular interactions in the repeat domain. At higher protein concentrations, potassium shifts from promoting intramolecular to intermolecular contacts. In line with this interpretation, Numata and colleagues have reported that kosmotropic ions induce oligomerization of the repeat domain at millimolar peptide concentrations[19]. It is noteworthy that we observe these effects despite the fact that the mini-spidroins likely favor solubility over phase separation due to the solubilizing effects of NT[35].

Potassium is likely to have a pronounced effect on phase transitions in native spidroins, considering their high number of repeats and extreme concentration in the gland. Recombinant mini-spidroins require high phosphate concentrations to undergo LLPS[13–15]. Importantly, spidroin droplets formed at high salt are metastable and undergo spontaneous aggregation, which would be detrimental in native silk dope[18]. We speculate that much lower amounts of kosmotropic ions would be required to promote LLPS-like interactions in the silk gland, where there is a higher concentration of repeat domains. MassFluidix MP, where interference from high amounts of KP_i is mitigated by rapid dilution, provides an indication of how LLPS could contribute to silk assembly. We find that pre-assembly of NT2RepCT^YF into macroscopic droplets reduces oligomeric intermediates when polymerization is triggered by lowering the pH. Considering the sensitivity to potassium that we observe with mini-spidroins in dilute solutions, we speculate that even a small shift in the potassium content of the gland may move the spidroins in their phase space to facilitate more efficient spinning.

Linder and co-workers have recently observed by analytical ultracentrifugation that NT2RepCT forms clusters that transition to aggregates as a function of protein concentration, temperature, or pH[36]. Their findings show that the protein occupies a two-phase regime even below the threshold for LLPS. The MP data now reveal that the tendency to oligomerize extends to the low nanomolar range, further blurring the distinction between single proteins, clusters, and droplets. Rather than presenting a phase diagram with a defined solubility line, spidroins are inherently bound to self-assemble via their repeat regions, which can be fine-tuned by ions. This behavior is markedly different from other phase-separating proteins. For example, MP has shown that LLPS of α-Synuclein does not proceed via small oligomers but is driven by the formation of megadalton clusters at micromolar protein concentrations[29]. We speculate that the ability to assemble spidroins with minimal intermediates helps spiders to achieve their high spinning speeds. Together with the recent demonstration that native spidroin dope is amenable to MP analysis[37], our study raises the possibility of following silk LLPS and assembly in real-time with single-molecule methodologies.

Materials and Methods

Protein sequences

NT2Rep 21820 Da	MGHHHHHHMSHTT PWTNPGLAENFMNSF MQGLSSMPGFTASQLD DMSTIAQSMVQSIQSLA AQGRTSPNKLQALNM AFASSMAEIAASEEG GGSLSTKTSSIASAMS NAFLQTTGVVNQPF INEITQLVSMFAQAG MNDVSAGNSGRGQ GGYGQGSGGNAA AAAAAAAAAAAA GQGGQGGYGRQS QGAGSAAAAAAAA AAAAAAGSGQGGY GGQGQGGYGQSGS
NT2RepCT^{YF}33100 Da	MGHHHHHHMSHTT PWTNPGLAENFMN SFMQGLSSMPGFTA SQLDDMSTIAQSMVQ SIQSLAAQGRTSPNK LQALNMAFASSMAE IAASEEGGGSLSTKT SSIASAMSNAFLQTT GVVNQPFINEITQLV SMFAQAGMNDVSA GNSGRGQGGFGQG SGGNAAAAAAAAA AAAAAGQGGQGG FGRQSQGAGSAAA AAAAAAAAAAGS GQGGFGGQGQGG FGQSGSVTSGGYG YGTSAAAGAGVAA GSYAGAVNRLSSA EAASRVSSNIAAIAS GGASALPSVISNIYS GVVASGVSSNEALIQ ALLELLSALVHVLSS ASIGNVSSVGVDST LNVVQDSVGQYVG
NT15006 Da	MGHHHHHHMSHTTP WTNPGLAENFMNSFM QGLSSMPGFTASQLDDM STIAQSMVQSIQSLAAQ GRTSPNKLQALNMAF ASSMAEIAASEEGGG SLSTKTSSIASAMSNA FLQTTGVVNQPFINEI TQLVSMFAQAGMNDVSA

Protein expression and purification

All proteins were expressed and purified as previously described, however sonication (6 min, 2 s on, 8 s off, 30%) was used for cell disruption[5,38]. NT2repCT^{YF} was dialyzed into deionized water while NT2rep and NT were kept in 20 mM Tris, pH 8. After concentrating (NT to 10 mM, NT2rep and NT2repCT^{YF} to 200 – 300 μM) using Amicon spin filters (Millipore), all proteins were stored at -20 °C.

Microscopy

Bright-field microscopy images of 10 μM NT2repCT^{YF} droplets in 20 mM or 500 mM KP$_i$, pH 8, were acquired using a Nikon Eclipse Ti series inverted microscope (Nikon) equipped with a Crest X-light V2 series confocal unit (Nikon) using a Plan Apo 40x objective (Nikon) and a Zyla sCMOS camera (Andor).

Thioflavin T assay

Aggregation kinetics were monitored by measuring the ThT fluorescence (excitation: 445-8 nm, emission: 488-15 nm) using a CLARIOstar microplate reader (BMG labtech) with the gain set to 2000. In black half-area 96-well polystyrene microplates with a transparent bottom (Corning), 40 μL 10 μM ThT and 25 μM NT2RepCT^{YF} were mixed in the different buffers (20 mM NaP$_i$ pH 8, 20 mM NaP$_i$ pH 5, 20 mM KP$_i$ pH 8, 20 mM KP$_i$ pH 5, 500 mM NaP$_i$ pH 8, 500 mM NaP$_i$ pH 5, 500 mM KP$_i$ pH 8, 500 mM KP$_i$ pH 5) and the plate sealed with transparent cover film to avoid evaporation. All measurements were conducted at 30 °C without agitation.

Mass photometry

All mass photometry experiments were carried out at room temperature using the Refeyn Two^{MP} instrument (Refeyn) in the normal measurement mode with regular image size. Proteins were pre-diluted first to 10 μM in 20 mM NaP$_i$ pH8 and from that further diluted (400 nM) into the desired buffer. A final concentration of 20 nM (NT2RepCT^{YF}, NT-2rep) or 100 nM (NT) was then used on the mass photometry slide. Each measurement was recorded for 1 min (3000 frames) using the AcquireMP (2024 R1.1) software. Histograms were created in DiscoverMP (v2024 R1) with β-amylase (56, 112, and 224 kDa) or bovine serum albumin (66 and 132 kDa) in 20 mM NaP$_i$ pH 8 as mass calibrants. Data were analyzed using DiscoverMP software (Refeyn). NT2RepCT measurements were performed at least in triplicate, and NT and NT2Rep measurements at least in duplicates. Representative examples of inter-experiment variation are shown in Fig. S5. Unbinding peak intensities were significantly lower than binding peak intensities in all instances.

Mass Fluidix

Mass Fluidix-MP measurements were carried out using 1st-generation microfluidic chips (Refeyn). 10 μM NT2RepCT^{YF} in 20 mM NaPi, pH 8, or in 500 mM KPi, pH 8, were pumped via the sample inlet. 20 mM NaPi, pH 8, or 20 mM NaPi, pH 5, were supplied *via* the buffer inlet. Inlet tubes were washed with MQ and primed with buffer before and between runs. Nitrogen pressure was used to control the sample and buffer flow. Pressure and related flow rates were adjusted manually using the OxyGEN software. Flow rates were adjusted to 1 μL/min and 999 μL/min for sample and buffer, respectively, resulting in 1500 - 3000 binding events/min. Histograms were created in DiscoverMP (v2024 R1), and β-amylase (56, 112, and 224 kDa) or bovine serum albumin (66 and 132 kDa) was used as mass calibrant.

Native ion mobility mass spectrometry

NT2RepCT^{YF} was buffer-exchanged into 100 mM ammonium acetate, or into 100 mM ammonium acetate supplemented with 10 mM sodium acetate (NaAc) or 10 mM potassium acetate (KAc), pH 8, using BioSpin6 columns (BioRad, CA, USA). Samples were loaded into nESI capillaries (Thermo Fisher Scientific Inc., MA, USA). Mass spectra were recorded in positive ionization mode on a Waters Synapt G1 traveling-wave IM mass spectrometer (MS Vision, The Netherlands). The capillary voltage was maintained at 1,5 kV, and the sample cone was 100 V. The source temperature was +30 °C. The trap and transfer collision energies were 50 V. The trap gas was argon at a flow rate of 1.5 mL/min, and the IMS gas was nitrogen at a flow rate of 18.5 mL/min. The ion mobility-mass spectrometry settings were: IMS wave height 10 V and IMS wave velocity 350 m/s. Data were analyzed using MassLynx 4.1 (Waters, UK).

Article

Data availability
All data are available from the corresponding authors upon reasonable request.

References

1. Hu, X. et al. Molecular Mechanisms of Spider Silk. *Cell. Mol. Life Sci.* **63**, 1986–1999 (2006).
2. Jin, H.-J. & Kaplan, D. L. Mechanism of Silk Processing in Insects and Spiders. *Nature* **424**, 1057–1061 (2003).
3. Kerkam, K., Viney, C., Kaplan, D. & Lombardi, S. Liquid Crystallinity of Natural Silk Secretions. *Nature* **349**, 596–598 (1991).
4. Vollrath, F. & Knight, D. P. Liquid Crystalline Spinning of Spider Silk. *Nature* **410**, 541–548 (2001).
5. Andersson, M. et al. Carbonic Anhydrase Generates CO2 and H+ That Drive Spider Silk Formation Via Opposite Effects on the Terminal Domains. *PLoS Biol.* **12**, e1001921 (2014).
6. Landreh, M. et al. A pH-Dependent Dimer Lock in Spider Silk Protein. *J. Mol. Biol.* **404**, 328–336 (2010).
7. Hagn, F., Thamm, C., Scheibel, T. & Kessler, H. pH-Dependent Dimerization and Salt-Dependent Stabilization of the N-terminal Domain of Spider Dragline Silk—Implications for Fiber Formation. *Angew. Chem. Int. Ed.* **50**, 310–313 (2011).
8. Askarieh, G. et al. Self-Assembly of Spider Silk Proteins Is Controlled by a pH-Sensitive Relay. *Nature* **465**, 236–238 (2010).
9. Hagn, F. et al. A Conserved Spider Silk Domain Acts as a Molecular Switch That Controls Fibre Assembly. *Nature* **465**, 239–242 (2010).
10. Andersson, M. et al. Biomimetic Spinning of Artificial Spider Silk from a Chimeric Minispidroin. *Nat. Chem. Biol.* **13**, 262–264 (2017).
11. Rising, A. & Johansson, J. Toward Spinning Artificial Spider Silk. *Nat. Chem. Biol.* **11**, 309–315 (2015).
12. Knight, D. & Vollrath, F. Changes in Element Composition along the Spinning Duct in a Nephila Spider. *Naturwissenschaften* **88**, 179–182 (2001).
13. Mohammadi, P. et al. Controllable Coacervation of Recombinantly Produced Spider Silk Protein Using Kosmotropic Salts. *J. Colloid Interface Sci.* **560**, 149–160 (2020).
14. Leppert, A. et al. Liquid–Liquid Phase Separation Primes Spider Silk Proteins for Fiber Formation via a Conditional Sticker Domain. *Nano Lett.* **23**, 5836–5841 (2023).
15. Malay, A. D. et al. Spider Silk Self-Assembly via Modular Liquid-Liquid Phase Separation and Nanofibrillation. *Sci. Adv.* **6**, eabb6030 (2020).
16. Slotta, U. K., Rammensee, S., Gorb, S. & Scheibel, T. An Engineered Spider Silk Protein Forms Microspheres. *Angew. Chem. Int. Ed.* **47**, 4592–4594 (2008).
17. Stengel, D. et al. Tyrosine's Unique Role in the Hierarchical Assembly of Recombinant Spider Silk Proteins: From Spinning Dope to Fibers. *Biomacromolecules* **24**, 1463–1474 (2023).
18. Leppert, A. et al. Controlling Drug Partitioning in Individual Protein Condensates through Laser-Induced Microscale Phase Transitions. *J. Am. Chem. Soc.* **146**, 19555–19565 (2024).
19. Oktaviani, N. A., Matsugami, A., Hayashi, F. & Numata, K. Ion Effects on the Conformation and Dynamics of Repetitive Domains of a Spider Silk Protein: Implications for Solubility and β-Sheet Formation. *Chem. Commun.* **55**, 9761–9764 (2019).
20. Landreh, M. et al. Liquid-Liquid Crystalline Phase Separation of Spider Silk Proteins. *Commun. Chem.* **7**, 260 (2024).
21. Greco, G. et al. Tyrosine Residues Mediate Supercontraction in Biomimetic Spider Silk. *Commun. Mater.* **2**, 43 (2021).
22. Young, G. et al. Quantitative Mass Imaging of Single Biological Macromolecules. *Science* **360**, 423–427 (2018).
23. Asor, R., Loewenthal, D., van Wee, R., Benesch, J. L. P. & Kukura, P. Mass Photometry. *Annu. Rev. Biophys.* **54**, 379–399 (2025).
24. Christofi, E. & Barran, P. Ion Mobility Mass Spectrometry (IM-MS) for Structural Biology: Insights Gained by Measuring Mass, Charge, and Collision Cross Section. *Chem. Rev.* **123**, 2902–2949 (2023).
25. Susa, A. C., Xia, Z. & Williams, E. R. Native Mass Spectrometry from Common Buffers with Salts That Mimic the Extracellular Environment. *Angew. Chem. Int. Ed. Engl.* **56**, 7912–7915 (2017).
26. Merenbloom, S. I., Flick, T. G., Daly, M. P. & Williams, E. R. Effects of Select Anions from the Hofmeister Series on the Gas-Phase Conformations of Protein Ions Measured with Traveling-Wave Ion Mobility Spectrometry/Mass Spectrometry. *J. Am. Soc. Mass Spectrom.* **22**, 1978–1990 (2011).
27. Claasen, M., Kofinova, Z., Contino, M., Struwe, W. B. Analysis of Protein Complex Formation at Micromolar Concentrations by Coupling Microfluidics with Mass Photometry. *J. Vis. Exp. Jo*VE No. 203. https://doi.org/10.3791/65772 (**2024**).
28. Yang, S. et al. Calcium Ion-Triggered Liquid-Liquid Phase Separation of Silk Fibroin and Spinning through Acidification and Shear Stress. *Nat. Commun.* **15**, 10394 (2024).
29. Ray, S. et al. Mass Photometric Detection and Quantification of Nanoscale α-Synuclein Phase Separation. *Nat. Chem.* **15**, 1306–1316 (2023).
30. Schwarze, S., Zwettler, F. U., Johnson, C. M. & Neuweiler, H. The N-Terminal Domains of Spider Silk Proteins Assemble Ultrafast and Protected from Charge Screening. *Nat. Commun.* **4**, 2815 (2013).
31. Landreh, M. et al. Mass Spectrometry Captures Structural Intermediates in Protein Fiber Self-Assembly. *Chem. Commun.* **53**, 3319–3322 (2017).
32. Wu, D. & Piszczek, G. Measuring the Affinity of Protein-Protein Interactions on a Single-Molecule Level by Mass Photometry. *Anal. Biochem.* **592**, 113575 (2020).
33. Wei, S.-P. et al. Formation and Functionalization of Membraneless Compartments in Escherichia Coli. *Nat. Chem. Biol.* **16**, 1143–1148 (2020).
34. Zhang, Y. et al. Cryo-EM Structures of Artificial Spider Silk Nanofibrils Reveal Insights into β Sheet Crystallization. *Cell Rep. Phys. Sci.* **6**, 102659 (2025).
35. Kaldmäe, M. et al. High Intracellular Stability of the Spidroin N-Terminal Domain in Spite of Abundant Amyloidogenic Segments Revealed by in-Cell Hydrogen/Deuterium Exchange Mass Spectrometry. *FEBS J.* **287**, 2823–2833 (2020).
36. Fedorov, D. et al. Metastable liquid–liquid phase separation and aging lead to strong processing path dependence in mini-spidroin solutions. *Adv. Funct. Mater.* **35**, 2410421 (2024).
37. Johnson, H. R. et al. Distinct dimerization mechanisms in silkworm and spider silk proteins revealed by mass photometry. *J. Phys. Chem. Lett.* **16**, 11451–11457 (2025).
38. Arndt, T. et al. Engineered spider silk proteins for biomimetic spinning of fibers with toughness equal to dragline silks. *Adv. Funct. Mater.* **32**, 2200986 (2022).

Acknowledgements

Author contributions
H.O. produced protein and performed MP and MS measurements, analyzed the data, and wrote the first draft of the manuscript. SSJ produced protein and contributed to MP measurements. B.S. and T.B.P. provided materials and expertise. J.L.P.B. contributed to MP optimization and data analysis. A.R., A.L., and M.L. designed the study and supervised experiments and data analysis. All authors commented on the final manuscript.

Competing interests

The authors declare no competing interests.

Additional information

Supplementary information The online version contains supplementary material available at https://doi.org/10.1038/s43246-025-01051-3.

Correspondence and requests for materials should be addressed to Anna Rising, Axel Leppert or Michael Landreh.

Peer review information *Communications Materials* thanks the anonymous reviewers for their contribution to the peer review of this work. A peer review file is available.

Reprints and permissions information is available at http://www.nature.com/reprints

Publisher's note Springer Nature remains neutral with regard to jurisdictional claims in published maps and institutional affiliations.